Considerations on the Numerical Modeling and Performance of Axial Swirlers Under Relight Conditions

Nicholas Grech[1]
e-mail: n.grech@cranfield.ac.uk

Charlie Koupper

Pavlos K. Zachos

Vassilios Pachidis

Riti Singh

Department of Power and Propulsion,
Cranfield University,
Bedfordshire, MK43 0AL, United Kingdom

Numerical modeling of aero engine combustors under relight conditions is a matter of continuously increasing importance due to the demanding engine certification regulations. In order to reduce the complexity and the cost of the numerical modeling, common practice is to replace the atomizer's swirlers with velocity profiles boundary conditions, very often scaled down from nominal operating conditions assuming similarity of the swirler flowfield. The current numerical study focuses on the flowfield characteristics of an axially swirled atomizer operating within a windmilling engine environment. The scalability of the velocity profile from higher power settings is examined. Observations on the performance of the axial swirler under relight conditions are also made. Experimental data was used as a validation platform for the numerical solver, after a grid sensitivity study and a turbulence model selection process. Boundary conditions for simulating the windmilling environment were extracted from experimental work. The swirler axial and tangential velocity profiles were normalized using the swirler inlet velocity. Results showed that both profiles are only scalable for windmilling conditions of high flight Mach number (≥ 0.5). At low flight Mach numbers, the actual profile had a lower velocity than that predicted through scaling. The swirl number was found to deteriorate significantly with the flight velocity following a linear trend, reducing significantly the expected flame quality. As a consequence the burner is forced to operate at the edge of its stability loop with low certainty regarding its successful relight. [DOI: 10.1115/1.4007132]

1 Introduction

An aero engine's relight capability is a critical step in the certification requirement, and a major challenge in terms of the combustor's design. Under subidle conditions, including altitude relight and windmilling, the air mass flow rate through the engine is very low. The compressors rotate at low speed (windmilling) or remain in a static condition (locked-rotor), creating a pressure drop rather than a pressure rise as demonstrated by Vincent et al. [1]. The conditions at the combustor inlet are therefore very different from nominal operation. Numerical methods often used to understand the phenomena that dominate the combustor's performance under far off-design conditions. This is due to their impact on the fuel spray's characteristics (Caines et al. [2], Beck et al. [3], and Kozaily et al. [4]) and, therefore, on the engine's relight capability.

To reduce the complexity of the combustor numerical model, the swirler geometry is often omitted. The flowfield is created using an inlet velocity profile boundary condition, scaled according to the operating condition being simulated. However, scaling of velocity profiles may introduce errors at conditions of very low air flow rate and low density—which are typical of altitude relight—due to low Reynolds number effects. It would be, therefore, useful to determine at which conditions velocity profile scaling is valid, due to the influence on the flame dynamics and stability, and the direct effect on assessing the engine's relight capability. The swirl number (S_N) characterizes the amount of rotation imparted to the axial flow by the swirler, indicating the intensity of the swirl which creates the recirculation zone. This recirculating flow improves the flame stability in the combustor and can reduce the flame length as shown in Fig. 1, thereby minimizing the combustor volume which is designed to meet the altitude relight criteria, but is otherwise oversized for nominal operating conditions. Though the swirl number depends on the swirler's geometrical design, Sheen et al. [5] have shown that, in the case of radial swirlers, conditions of low flow reduce the swirl number. This will have a direct influence on the flow field, reducing the swirl intensity and changing the nature of the recirculation zone, as shown by Chatterjee et al. [6]. A correlation that predicts the swirl number in terms of the swirler's inlet conditions at windmilling would predict the intensity and reverse flow magnitude of the flowfield during an altitude relight, in an attempt to minimize the combustor volume while maintaining flame stability. This is obviously desirable since large combustors require more cooling flow, are heavier and increase shaft lengths.

2 Swirler Aerodynamics

To reduce the inlet flow velocity enough to achieve adequate flame stability, the primary-zone inlet includes some form of swirl. Imparting a high rotation to the incoming flow, radial and axial pressure gradients are created. In strongly swirling flows, the adverse pressure gradient is enough to induce flow reversal. This phenomenon, known as vortex breakdown, creates a toroidal flow reversal which mixes with the incoming air and fuel. The recirculated mass flow rate increases with the swirl magnitude [7,8]. The degree of swirl is expressed in terms of the swirl number (S_N). Huang and Yang [9] and Palies et al. [10] underline the impact of the swirl strength on the flame dynamics, with high swirl numbers increasing the turbulence intensity and flame speed, shortening the flame length. The net heat release is unchanged due to the enhanced flame speed.

A detailed review on swirling flows can be found in Beer and Chigier [11], Gupta et al. [12], Sloan et al. [7] and Lefebvre [13],

[1]Corresponding author.

Contributed by the Gas Turbine Institute (IGTI) of ASME for publication in the Journal of Engineering for Gas Turbines and Power. Manuscript received June 26, 2012; final manuscript received July 10, 2012; published online September 28, 2012. Editor: Dilip R. Ballal.

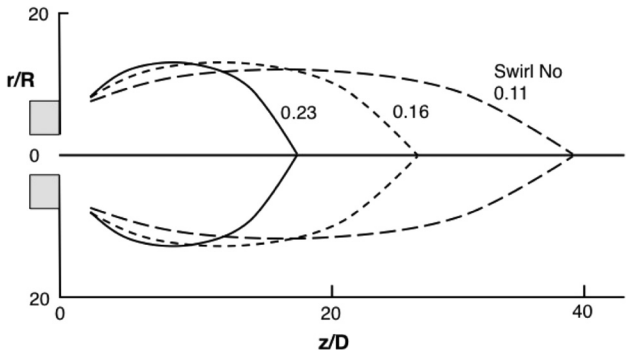

Fig. 1 Effect of swirl number on the flame front [14]

while more experimental and prediction work is found in Lilley [14,15]. The present study investigates the flow field characteristics of an axial swirler, operating within a windmilling engine environment, relative to nominal operating conditions, using CFD. The flow's swirl number is also monitored for changes with the flight conditions. These results can give an indication of the subidle flame characteristics, since as stated in Lilley [14], the phenomena observed and measured in nonreacting flows were found to be similar in swirling flames. The numerical solver is first validated against experimental data by Kilik [8]. A brief overview of a number of studies which compare experimental and numerical results of swirling flows, is also included.

3 Numerical Modeling of Swirling Flows

Previous studies, using a variety of turbulence models, have attempted to capture the swirling flow field as accurately as possible against experimental data. Widmann et al. [16] studied the isothermal airflow through a radial 12-vane-cascade swirl generator, comparing the k-ε standard and renormalization group (RNG) models of which the former proved inadequate in predicting the outlet velocity profile. The swirl number from the numerical simulation underpredicts by 50% the value estimated by the geometry based correlations [11]. The standard k-ε model gave inaccurate predictions in the work of Brum and Samuelsen [17], with large underestimations of the axial velocity on the center line and poor prediction of the central toroidal recirculation zone (CTRZ) length and turbulence intensity. Radial profiles of axial velocity, match well with the experimental, except in regions close to the swirler exit. The tangential velocity is well predicted in terms of profile shape, but overpredicted by $\simeq 20$ to 45%. Davoudzadeh et al. [18], using a Reynolds-averaged Navier-Stokes (RANS) k-ε *Shih* model [19] found that the axial velocity profile on the center line is well predicted, but the CTRZ length is overpredicted by $\simeq +60\%$. The maximum CFD overestimation of a velocity peak magnitude is $\simeq \times 2.1$ relative to experimental data.

Escue and Cui [20], in an attempt to reproduce the experimental results by Rocklage-Marliani et al. [21], use both k-ε RNG and Reynolds stress model (RSM). Radial profiles of axial and tangential velocity are better captured by the k-ε RNG model. However RSM provides better results as the swirl number increases as the flow is more anisotropic. Weber et al. [22] also show better agreement of the RSM model with experimental data. Turbulence kinetic energy decays unrealistically for both the k-ε RNG and RSM models [20]. Concluding, using RANS modeling, over/understimation of peak values by 20–45% in the velocity profiles is common, and turbulence levels (intensity and kinetic energy) are very poorly predicted. The k-ε realizable turbulence model is rarely used, even though Mongia [23], found it to match the experimental results best, among the k-ε variants, k-ω and RSM turbulence models. Results from large eddy simulation (LES) and direct numerical simulation (DNS) models are in better agreement with the experimental measurements relative to RANS [24,25,26], even though unsteady RANS RSM results gave good agreement with LES and experimental data [27].

4 Validation of Numerical Solver

4.1 Numerical Model Setup. Steady and incompressible simulations were run with ANSYS Fluent, with QUICK discretization. The experimental setup described in Kilik [8] was replicated in the numerical domain. The vanes' edge profiles (both inlet and outlet) and sharpness, were not available, while differences due to manufacturing tolerances for the experimental work, may also impact the results.

A fully annular domain was used. The swirler (designated S9) consists of 16 curved vanes, with an aspect ratio of 0.4, 24.3 mm vane chord length and swirler outer diameter D_{sw} of 76.2 mm (refer to Fig. 2). A flat-vaned swirler was also tested (designated S6), having an aspect ratio of 0.4, 25.4 mm vane chord length, and outer diameter similar to S9. The vanes were set with an inlet angle of 0 deg and outlet angle of 50 deg for S9 and 60 deg for S6, relative to the axis of the swirler. Vane thickness was set at 1 mm. The swirl number, estimated from swirler geometry, is given as 1.04 for S9 and 1.51 for S6 [8]. The swirler exhausts into a cylindrical domain which, for the validation work, was set as a "pressure outlet" since the experimental data was taken from an unconfined swirler setup. A "pressure outlet" boundary condition was found to give better results than "outflow" (used at the outlet of open channel flows to model flow exits, where the details of the flow velocity and pressure are not known prior to solving the flow problem [28]) relative to the experimental measurements. The operating condition was set to atmospheric pressure, with a mass flow inlet of 0.06169 kg/s (0.136 lb/s) resulting in an axial velocity of 23.77 m/s at the swirler face, this also being the value specified for the experimental setup [8]. The total pressure drop (ΔP) across the swirler was measured and defined by Kilik [8] as the difference between swirler inlet total pressure (P_i) and atmospheric pressure (P_{atm}). The static pressure drop (Δp) was measured along the swirler central axis.

4.2 Grid Independency. A hex-core (tetrahedral cells on the walls, hexahedral cells in the remaining volume) unstructured mesh was used, as illustrated in Fig. 3. Wall functions were used instead of resolving the boundary layer; thus a y^+ of 30–45 was used on the vane surfaces, as suggested in Ref. [28]. This value of y^+ was maintained for all the models run. A number of different meshes with increasing density were run until a finer mesh resulted in no significant change in the results. The selected mesh

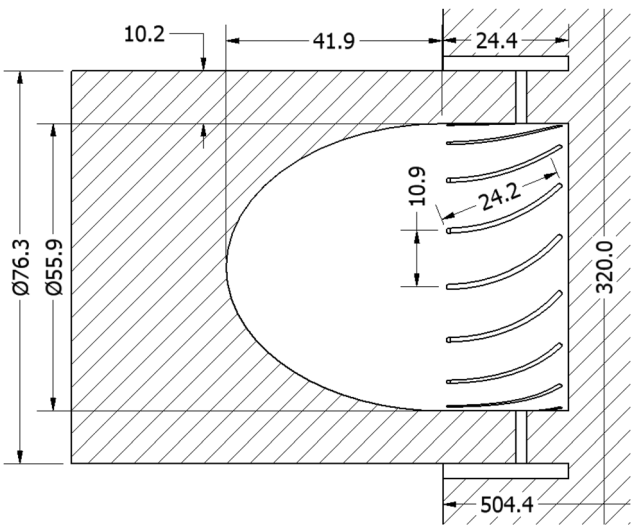

Fig. 2 Swirler dimensions (mm)

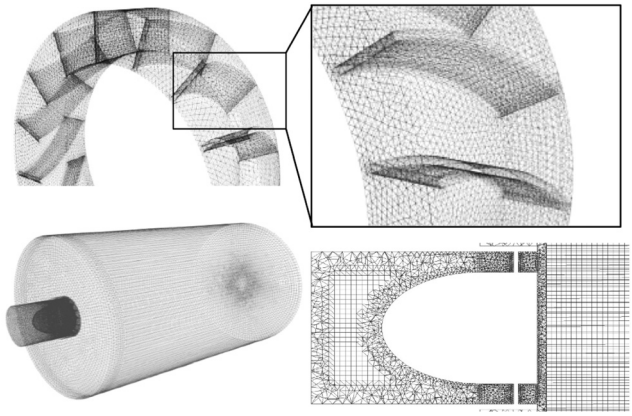

Fig. 3 Hex-core unstructured mesh

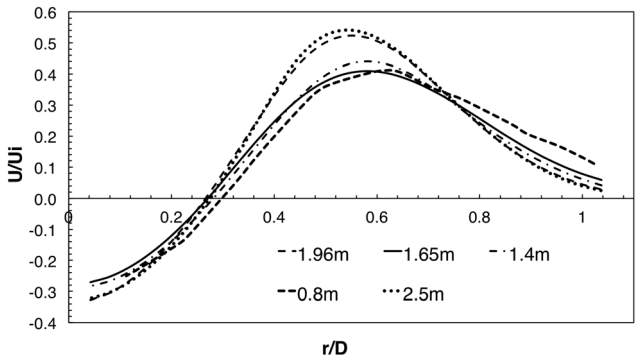

Fig. 4 Grid independency study

has 1.96×10^6 elements with the finer 2.5×10^6 and 4.3×10^6 element meshes showing no change in the velocity profiles, as shown in Fig. 4.

4.3 Selection of Turbulence Model. Since it is difficult to determine beforehand which turbulence model will produce the best agreement with the experimental results, a number of RANS turbulence models were tested, namely: k-ε RNG and realizable, standard k-ω and RSM. The standard k-ε model was not considered since it is known to predict swirling flowfields poorly, mainly because it neglects the anisotropic viscosity, and the generation of additional turbulence due to the effect of streamline curvature, as mentioned in Chatterjee et al. [6] and reported in Widmann et al. [16]. The two-equation k-ε models all suffer from limitations due to the isotropic eddy viscosity assumption (Boussinesq hypothesis), whereas swirling flows are anisotropic. The validation is based on the agreement with experimental measurements of: axial and tangential velocity profiles, total and static pressure drop across the swirler, and the size and shape of the CTRZ. Despite repeated efforts, a fully converged 2nd order solution using RSM could not be obtained, even after starting from a converged 1st order solution, and thus any RSM results shown are from the converged 1st order RSM solution only. The turbulence intensity was varied between 2–10% with no change in the circumferentially averaged velocity profiles, agreeing with Wang et al. [24] were it is demonstrated that up to 25% turbulence intensity, there is no effect on the swirling flow pattern.

4.3.1 Recirculation Zone Boundary. In terms of the reverse flow zone boundary (defined as the locations where $U = 0$), the k-ε realizable model results agree very well with the experimental points as shown in Fig. 5, having a maximum error of around 2%, for both zx and zy planes. The k-ω model also predicts the

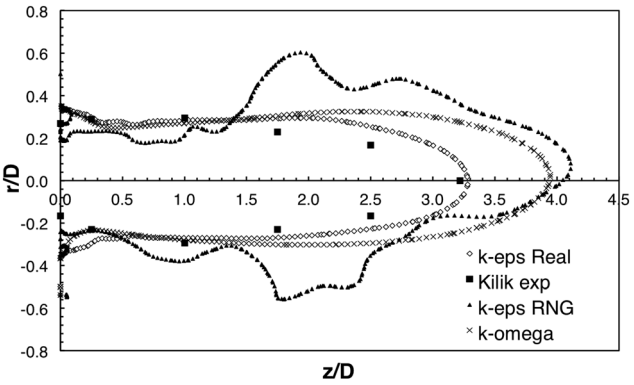

Fig. 5 Predicted recirculation zone boundary

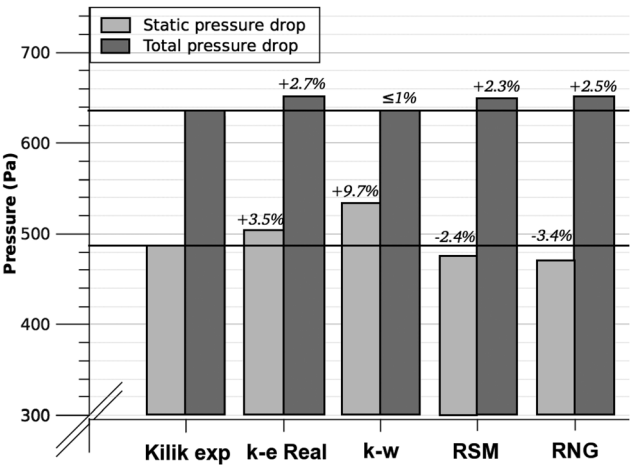

Fig. 6 Total and static pressure losses

Table 1 Numerical vs experimental [8] results

	CTRZ length (mm)	Mass flow (kg/s)
Kilik [8]	244	0.06168
k-ε realizable	248 (+1.6%)	0.06167 (−0.1%)
k-ε RNG	306 (+25.4%)	0.06061 (−1.7%)
k-ω	301 (+23.4%)	0.0592 (−4.0%)
RSM	358 (+46.7%)	0.0586 (−5.0%)

boundary quite well, but overpredicts its length. The k-ε RNG is also unsuitable.

4.3.2 Pressure Drop, Mass Flow and Velocity Profiles. As shown in Fig. 6, all the models provide a good estimate of both static and total pressure loss, with most errors being below 4% relative to experimental. Only the k-ω model overestimates significantly the static pressure drop. In terms of the mass flow prediction, Table 1 shows that the percentage errors are very small for both k-ε realizable and RNG models. The circumferentially averaged and normalized velocity profiles, shown in Fig. 7, again indicate that the k-ε realizable model produces results which align best with the experimental data. The axial velocity profiles are well captured by the numerical solver, even at far downstream positions. The tangential velocity is predicted relatively well close to the swirler, but far downstream, the magnitude is underpredicted.

4.3.3 Swirl Number. The swirl number characterizes the swirl intensity. Generally, values above 0.6 indicate a strongly swirling

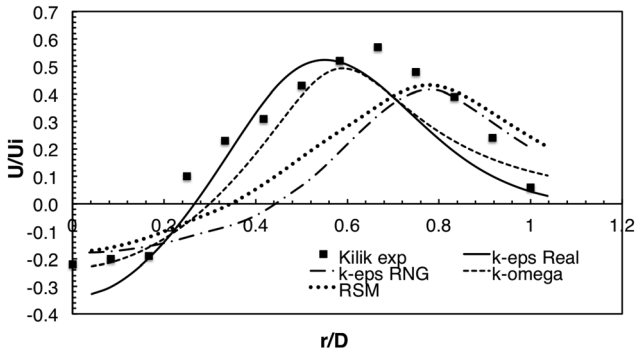

Fig. 7 Normalized velocity profiles

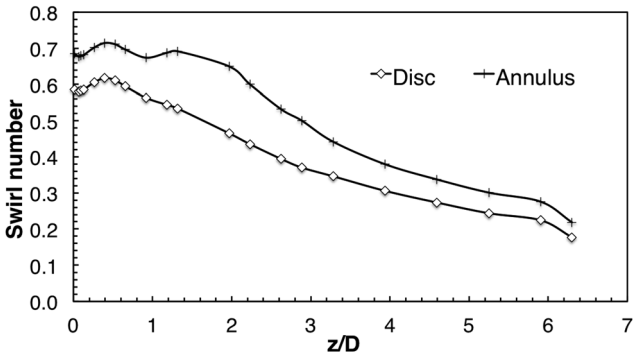

Fig. 8 Swirl number deterioration

flow. Theoretically, the swirl number can be estimated from the flow parameters using Eqs. (1), (2) and (3) as described by Gupta et al. [12].

$$S_N = \frac{2G_\varphi}{G_x D_{sw}} \tag{1}$$

where G_φ is the axial flux of swirl momentum, and G_x is the axial flux of axial momentum, as defined in the following equations:

$$G_\varphi = 2\pi \int_0^{R_{sw}} \left(\rho UW + \rho\overline{U'W'}\right) r^2 dr \tag{2}$$

$$G_x = 2\pi \int_0^{R_{sw}} \left(\rho U^2 + \rho\overline{U'^2} + (p - p_{\text{atm}})\right) r dr \tag{3}$$

Omitting the turbulent shear stresses $\rho\overline{U'W'}$ in Eq. (2) and $\rho\overline{U'^2}$ in Eq. (3), the derivation by Rose [29], and Chigier and Chervinsky [30], described in detail by Beer and Chigier [11], and Sloan et al. [7], gives:

$$G_\varphi = 2\pi \int_0^{R_{sw}} UW\rho r^2 \mathrm{d}r \tag{4}$$

$$G_x = 2\pi \int_0^{R_{sw}} \left(\rho U^2 + (p - p_{\text{atm}})\right) r dr \tag{5}$$

For vanes mounted on a central hub, the integrals of the equations change, as shown in Eq. (6).

$$G_\varphi = 2\pi \int_{R_h}^{R_{sw}} UW\rho r^2 \mathrm{d}r \tag{6}$$

The integral limits in Eq. (6) and the definition of the swirl number were found to vary, as highlighted by Sloan et al. [7]. Generally it is more common for the swirl number to be predicted using correlations based on the swirler's geometrical parameters. For an axial swirler, Eq. (7) is most commonly used, of which derivation is outlined in Beer and Chigier [11].

$$S_N = \frac{2}{3}\left[\frac{1 - (D_h/D_{sw})^3}{1 - (D_h/D_{sw})^2}\right] \tan\alpha \tag{7}$$

One should note that all the geometric correlations used to estimate the swirl number S_N are usually based on assumptions and simplifications, such as inviscid flow, uniform axial velocity distribution, negligible swirl momentum losses, and even omission of the pressure term in Eq. (5). Additionally, the velocity profiles created by various swirlers can lead to very different flow patterns, but with the same swirl strengths (i.e., S_N). When uncoupled from its velocity distributions S_N is therefore no more than an indication of the relative swirl intensity for a particular swirler [7].

Experimental work on radial-type swirlers by Sheen et al. [5], shows that the degree of swirl is dependent on the flow's Reynolds number (defined using the volumetric mean axial velocity and the diameter of the circular bluff body). For the same vane geometry, the swirl number was found to increase with Reynolds number while for Re $>$ 3000, the swirl number was found to be independent of it. This is of significant importance for the current study since under windmilling conditions, the swirler Reynolds number is likely to be very small due to the low air flow rates and pressure. The swirl number, calculated using Eq. (1) at several positions along the swirler axis, starts from a value of approximately 0.7, as illustrated in Fig. 8. Therefore, the geometrical correlation (which in Ref. [8] gives a value of 1.04) tends to over-predict the swirl number, as mentioned and explained in Widmann et al. [16]. The swirl number decays with the distance downstream, and this decay is also similar to the one reported in Ref. [16].

On the basis of the above validation exercise, the k-ε realizable turbulence model was selected and used for the rest of the study. It is important to mention that the experimental velocity profiles are based on measurements taken from a single point at each radial position, and have a 15% repeatability error [8]. It is, therefore, likely, that the experimental measurements were taken in regions of local maxima or minima, and thus do not represent the overall averaged velocity profile. The numerical data from the CFD is circumferentially averaged, and therefore for better comparison, Fig. 9 shows both the repeatablity error for the experimental work, and the maximum, minimum and circumferentially averaged velocities found at each radial position.

5 Simulations at Windmilling Conditions

With the numerical solver validated, the domain was converted to a confined configuration (representing the swirler within a combustor volume with walls) and run at subidle windmilling conditions. Experimental data in terms of total pressure tappings from various stations inside a turbojet engine, are presented by Vincent et al. [1]. These were derived from simulated conditions inside an altitude test rig. An estimate for the combustor's boundary conditions under windmilling conditions is found in Read [31], and assumes that half the inlet dynamic head is lost in the compressor. As illustrated in Fig. 10, the assumption is valid up to a flight Mach 0.5, above which the results diverge from the experimental measurements. These characteristics however depend on the accessories attached to the compressor. Additionally, while the cold total pressure loss across the combustor is assumed to remain constant [31] at around 5%, this was found to vary from 1%–10% with flight Mach number. For this study, the experimental measurements at windmilling conditions were used (see Table 2). The boundary conditions used for the groundstart simulations were taken from experimental pressure readings from a modern civil high-bypass turbofan start just before ignition. This was done by taking the reading just before a step increase in the combustion chamber pressure is noticed, which indicates that ignition has occurred.

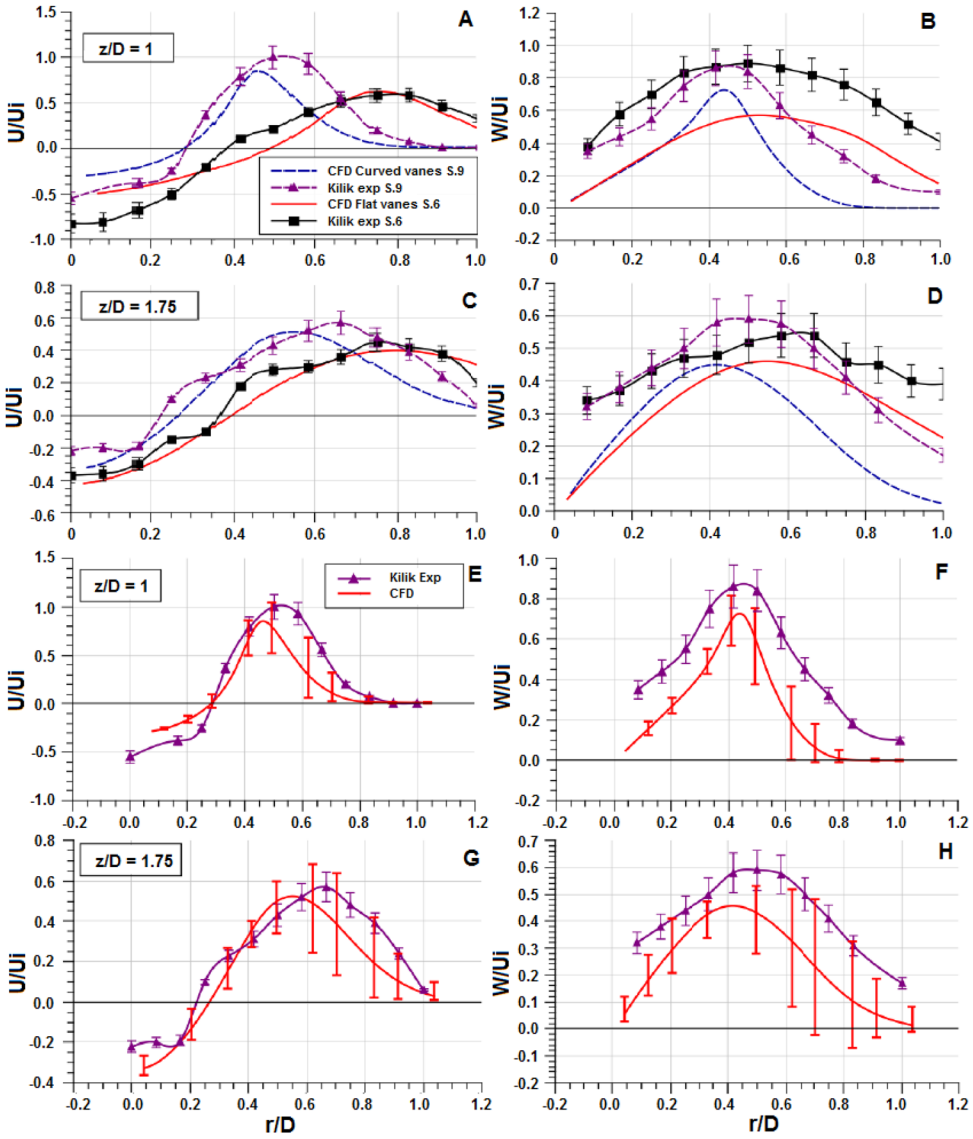

Fig. 9 Numerical versus experimental profiles: flat and curved vanes

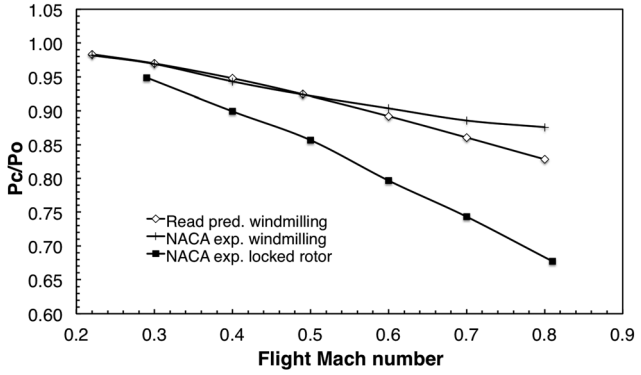

Fig. 10 Windmilling boundary conditions

Table 2 Subidle boundary conditions

		Windmilling alt. 9144 m				
	Groundstart (exp. data)	M0.8	M0.7	M0.6	M0.49	M0.4
P_c (kPa)	394.9	40.1	36.9	34.7	32.8	31.8
P_t (kPa)	375.2	36	35	33.1	32	31.3
T_c (K)	473	287	273	262	251	243
U_i (m/s)	87.1	108.8	71.6	63.1	43.4	36.3

6 Results and Discussion

6.1 Velocity Profiles and Scalability. The axial velocity distribution (Fig. 11) indicates a decay in the central recirculation zone strength, deteriorating from −45 m/s at flight Mach 0.8, to −15 m/s for flight Mach 0.4. Similar trends are observed in the axial (U) and tangential (W) velocity profiles (Figs. 12(*a*)–12(*d*)). The velocity profiles were normalized using the swirler inlet velocity (U_i). Such profiles (Figs. 12(*e*)–12(*h*) and Fig. 13), converge towards a single curve except for the low flight Mach number cases. This suggests that the low Reynolds number in the latter conditions has a significant influence, with the fluid viscosity becoming more dominant. This seems to occur at $\mathrm{Re}_{\mathrm{vane}} < 11,500$, as defined using the vane span, and shown in Fig. 14. It is standard practice to run experimental tests at nominal conditions, and scale the parameters down to the operating condition of interest [32]. Results in

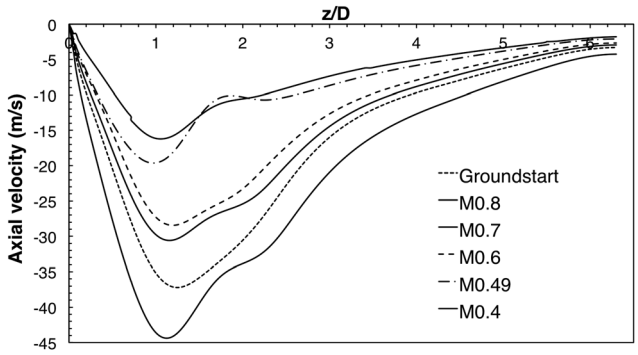

Fig. 11 Axial velocity along swirler axis

Figs. 12(*e*)–12(*h*) show that for high flight Mach number cases, axial and tangential profiles can be scaled with good accuracy when normalized. For low flight Mach numbers, the velocity profiles are not scalable.

6.2 Swirl Number. The swirl number was calculated using the parameters extracted from the numerical solution. As illustrated in Fig. 15, relative to the groundstart case, the value at the swirler face is very low, suggesting a swirling flow of weak intensity, corresponding to a reduction in recirculating mass flow as shown in Fig. 11 and experimentally verified by Kilik [8]. As previously mentioned, this reduction in swirl number will impact the flame dynamics, reducing the flame speed and increasing its length (refer to Fig. 1), possibly reducing the flame stability due to the low level of turbulence, recirculation and mixing with incoming air and fuel. The swirl number decays gradually with the distance downstream, until it attains a value similar to the groundstart condition. A correlation between the swirl number

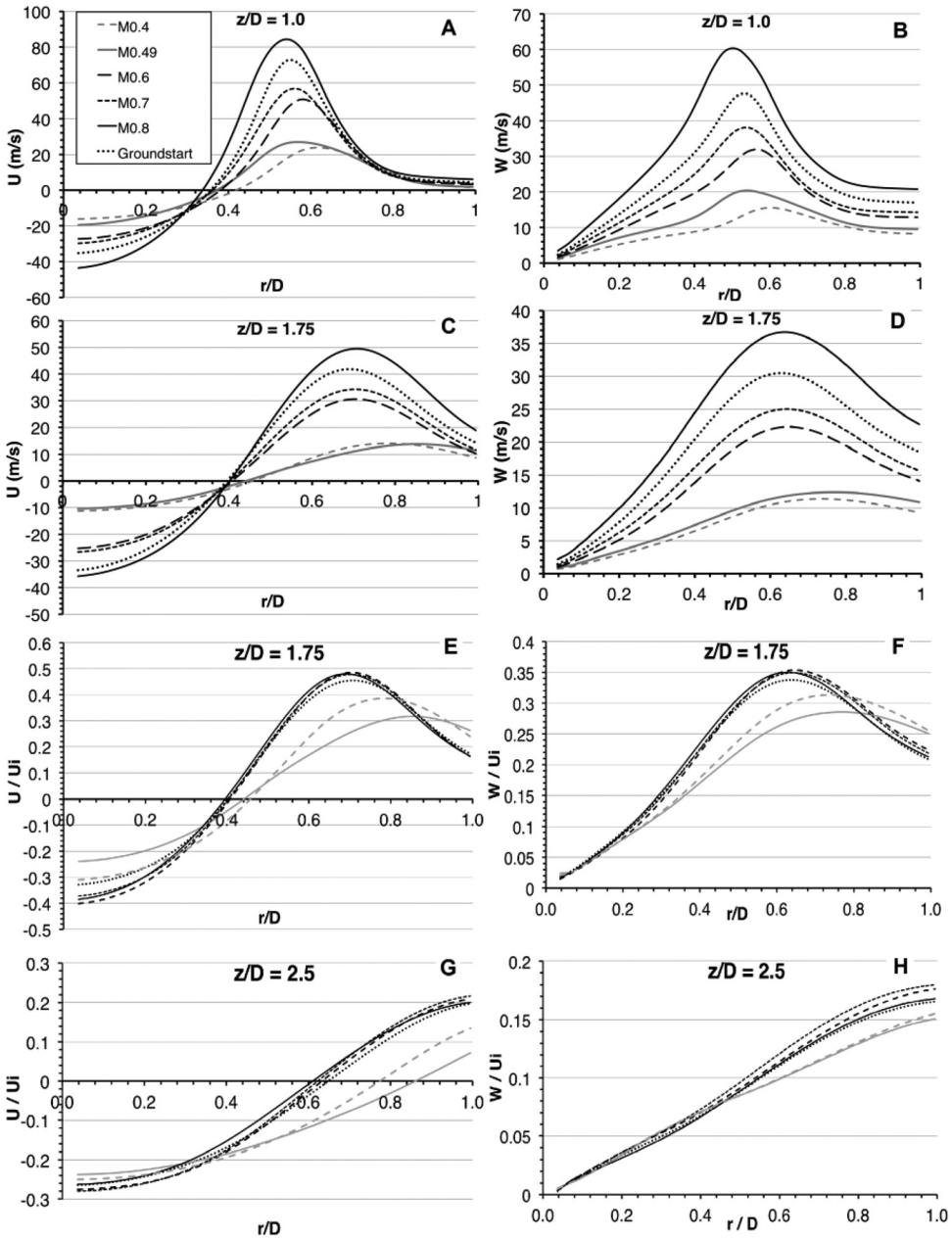

Fig. 12 Subidle velocity profiles

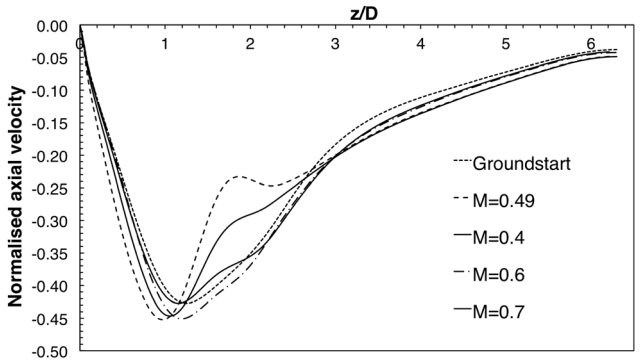

Fig. 13 Normalized axial velocity along swirler axis

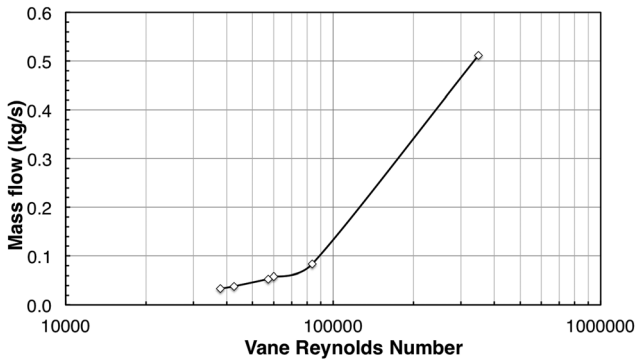

Fig. 14 Vane Reynolds number

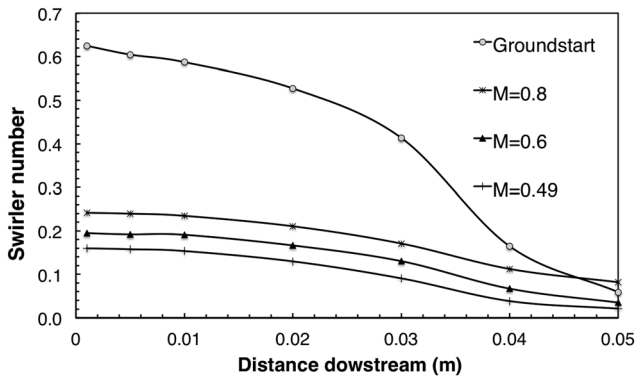

Fig. 15 Swirl number for subidle conditions

and the swirler inlet conditions was derived. The swirl number was found to be linearly related to the swirler inlet dynamic head, divided by the domain inlet total pressure relative to the free stream conditions. The swirl number will continue to increase with this parameter until it reaches the original design value. The correlation given in Eq. (8), gives an r^2 of 0.998 and RMSE of 0.0018 (see Fig. 16). In a more general form, a and b are characteristic of the swirler, Eq. (8) can be written as Eq. (9).

$$S_N = -0.0189 + 1.2208\left(\frac{0.5\rho U_i^2}{P_c - p_{\text{atm}}}\right) \tag{8}$$

$$S_N = a + b\left(\frac{0.5\rho U_i^2}{P_c - p_{\text{atm}}}\right) \tag{9}$$

This relation shows that for low power conditions, the swirl intensity is not a constant value that can be simply predicted from

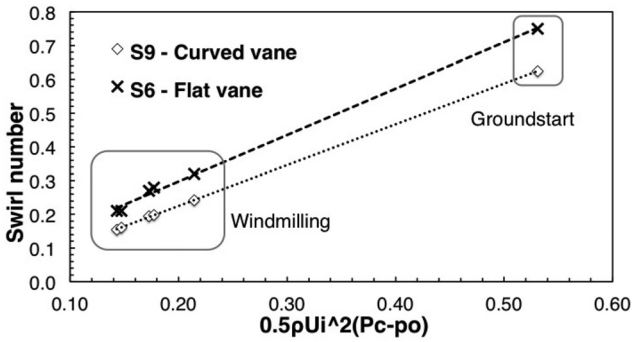

Fig. 16 Swirl number correlation for subidle conditions

the geometrical correlations, but is highly dependent on the operating conditions. The general application of the correlation for similar swirler designs was verified by simulating the flat vaned swirler (S6) under the same windmilling conditions, as shown in Fig. 16. The measured swirl number shows a similar, linear relationship with the swirler inlet dynamic head. The groundstart swirl number for both swirlers also fits in this relationship demonstrating its applicability for any subidle condition and its use in predicting the changes in flame characteristics at subidle. The simulations show a reduced rotation imparted by the swirler to the flow under conditions of low mass flow rate.

This results in low tangential velocities and a weak swirl under subidle conditions, reducing the adverse pressure gradient required by the flow to create a reverse flow region. The effect is visible in Fig. 11. The velocity magnitude of the reversing flow is reduced, suggesting a recirculation zone of weaker intensity and low reverse mass flow rate. The study also demonstrates that using scaled velocity profiles for numerical simulations were the swirler is not included, is valid except under low flight speed windmilling conditions. In such cases, low Reynolds number effects influence the velocity profile. In practical terms, the results achieved show that for relight simulations at high flight Mach numbers, the swirler geometry can be omitted and substituted with a scaled velocity profile.

7 Conclusions

Numerical simulations were run to study the swirler flow field under subidle conditions. The solver was first validated against experimental data under atmospheric and unconfined conditions. The model was then subjected to total pressure boundary conditions obtained from experimental data of a windmilling engine operating at various flight Mach numbers. Results from the simulations provided the following conclusions:

- The k-ε realizable model was found to best capture the swirling flow relative to the experimental measurements in terms of: the axial and tangential velocity profiles, static and total pressure drops, air mass flow rate, and the boundary and shape of the reverse flow region. Turbulence kinetic energy was not accurately predicted.
- For subidle conditions, normalized flow fields were found to be similar except for flight Mach numbers of 0.4 and 0.49 were the vane Reynolds number was less than 11,500. This indicates that the flow field is scalable within a reasonable degree of accuracy when $Re_{vane} \geq 11,500$ and therefore complex combustor simulations can be simplified by applying the scaled velocity profiles as inlet boundary conditions. This however cannot be done for lower vane Reynolds numbers.
- The swirl number at the swirler face for the windmilling cases was found to be much smaller than the validation and groundstart cases. Both the grounstarting and validation case feature similar swirl numbers at the swirler exit. For windmilling, this value is approximately 65% lower, indicating a large

decay of the swirl intensity at such conditions. The reduction in swirl number is accompanied by a weaker recirculation zone, as demonstrated by the lower velocity magnitudes of the reversing flow along the central axis.

- A linear correlation exists between the swirl number and the swirler inlet conditions, providing a relatively accurate prediction (RMSE of 0.0018 and r^2 of 0.998). The correlation's applicability to single-annular swirlers of similar design was verified through simulations of a second flat-vaned swirler. Results from groundstart simulations of both swirlers also agree with the correlation's prediction, demonstrating its validity for subidle operations. The dependency of the flame dynamics on the swirl number makes such a correlation useful for determining the expected dynamics of the flame under altitude relight conditions.

Acknowledgment

The authors thank Rolls-Royce plc, in particular A. Rowe, S. Brown, R. Tunstall, and M. Zedda, for their support.

Nomenclature

CTRZ = central toroidal recirculation zone
D = diameter (mm)
DNS = direct numerical simulation
LES = large eddy simulation
P = total pressure (kPa)
p = static pressure (kPa)
r = radial distance (mm)
R = radius (mm)
Re = Reynolds number
RSM = Reynolds stress model
RANS = Reynolds averaged Navier Stokes
RMS = root mean square
RNG = renormalization group
S_N = swirl number
U = axial velocity (m/s)
W = tangential velocity (m/s)
z = distance along swirler axis (mm)

Subscripts

atm = atmospheric value
vane = swirler vane
c = compressor exit value
sw = swirler outer diameter
h = swirler inner diameter (hub)
i = vane inlet
n = upstream of swirler
t = turbine inlet value

Greek Symbols

α = swirler vane angle (deg)
Δ = difference or drop
ρ = density (kg/m^3)
μ = dynamic viscosity ($Pa \cdot s$)

References

[1] Vincent, K., Huntely, S., and Wilsted, H., 1952, "Comparison of Locked-Rotor and Windmilling Drag Characteristics of an Axial-Flow-Compressor Type Turbo Jet Engine," National Advisory Committee for Aeronautics, Tech. Report RM E51K15.

[2] Caines, B., Hicks, R., and Wilson, C., 2001, "Influence of Sub-Atmospheric Conditions on the Performance on an Airblast Atomizer," Proceedings of 37th AIAA/ASME/SAE/ASEE Joint Propulsion Conference and Exhibit, Salt Lake City, UT, July 8–11, Paper No. AIAA-2001-3573.

[3] Beck, J., Lefebvre, A., and Koblish, T., 1989, "Airblast Atomiztion at Conditions of Low Air Velocity," 27th Aerospace Sciences Meeting, Reno, NV, January 9–12, Paper No. AIAA-1989-0217.

[4] Kozaily, J., Zachos, P., Pachidis, V., and Singh, R., 2009, "Gas Turbine Fuel Atomisation Dynamics Under Sub-Atmospheric Conditions," XIX International Symposium on Air Breathing Engines 2009 (ISABE 2009), Montreal, Canada, September 7–11, Paper No. ISABE-2009-1160, pp. 502–510.

[5] Sheen, H., Chen, W., Jeng, S., and Huang, T., 1996, "Correlation of Swirl Number for a Radial-Type Swirl Generator," Exp. Therm. Fluid Sci., **12**, pp. 444–451.

[6] Chatterjee, D., Datta, A., Ghosh, A., and Som, S., 2004, "Effects of Inlet Air Swirl and Spray Cone Angle on Combustion and Emission Performance of a Liquid Fuel Spray in a Gas Turbine Combustor," J. Inst. Eng. AS (India), **85**, pp. 41–46.

[7] Sloan, D., Smith, P., and Smoot, D., 1986, "Modeling of Swirl in Turbulent Flow Systems," Progress in Energy and Combustion Science, **12**(3), pp. 163–250.

[8] Kilik, E., 1976, "The Influence of Swirler Design Parameters on the Aerodynamics of the Downstream Recirculation Region," Ph.D. thesis, Cranfield Institute of Technology, Cranfield, Bedfordshire, UK.

[9] Huang, Y., and Yang, V., 2005, "Effect of Swirl on Combustion Dynamics in a Lean-Premixed Swirl-Stabilized Combustor," Proc. Combust. Inst., **30**, pp. 1775–1782.

[10] Palies, P., Durox, D., Schuller, T., and Candel, S., 2011, "Experimental Study on the Effect of Swirler Geometry and Swirl Number on Flame Describing Functions". Combust. Sci. Technol., **183**, pp. 704–717.

[11] Beer, J., and Chigier, N., 1972, *Combustion Aerodynamics*, Applied Science Publishers Ltd., London.

[12] Gupta, A., Lilley, D., and Syred, N., 1984, *Swirl Flows*, Abacus Press, Tunbridge Wells, England.

[13] Lefebvre, A., 1999, *Gas Turbine Combustion*, 2nd ed., Taylor & Francis, New York.

[14] Lilley, D., 1977, "Swirl Flows in Combustion: A Review," AIAA J., **15**(8), pp. 1063–1078.

[15] Lilley, D., 1985, "Investigations of Flowfields Found in Typical Combustor Geometries," NASA Contractor Report No. 3869.

[16] Widmann, J., Charagundla, S., and Presser, C., 2000, "Aerodynamic Study of a Vane-Cascade Swirl Generator," Chem. Eng. Sci., **55**(22), pp. 5311–5320.

[17] Brum, R., and Samuelsen, G., 1982, "Two-Component Laser Anemometry Measurements in a Non-Reacting and Reacting Complex Flow Model Combustor," Western States Section/The Combustion Institute, Sandia National Laboratories, Livermore, CA.

[18] Davoudzadeh, F., Liu, N., and Moder, J., 2006, "Investigation of Swirling Air Flows Generated by Axial Swirlers in a Flame Tube," NASA Glenn Research Centre, Tech. Report No. TM-2006-214252.

[19] Shih, T., Liou, W., Shabbir, A., Yang, Z., and Zhu, J., 1995, "A New k-ε Eddy Viscosity Model for High Reynolds Number Turbulent Flows," Comput. Fluids, **24**(3), pp. 227–238.

[20] Escue, A., and Cui, J., 2010, "Comparison of Turbulence Models in Simulating Swirling Pipe Flows," Appl. Math. Model., **34**(10), pp. 2840–2849.

[21] Rocklage-Marliani, G., Schmidts, M., and Ram, I. V., 2003, "Three-Dimensional Laser-Doppler Velocimeter Measurements in Swirling Turbulent Pipe Flow," Flow, Turbul. Combust., **70**, pp. 43–67.

[22] Weber, R., Visser, B., and Boysan, F., 1990, "Assessment of Turbulence Modeling for Engineering Prediction of Swirling Vortices in the Near Burner Zone," Int. J. Heat Fluid Flow, **11**(3), pp. 225–235.

[23] Mongia, H., 2008, "Recent Progress in Comprehensive Modelling of Gas Turbine Combustion," Proceedings of 46th AIAA Aerospace Sciences Meeting and Exhibit, Reno, NV, January 7–10, Report No. AIAA-2008-1445.

[24] Wang, S., Yang, V., Hsiao, G., Hsieh, S., and Mongia, H., 2007, "Large-Eddy Simulations of a Gas Turbine Swirl Injector Flow Dynamics," J. Fluid Mech., **583**, pp. 99–122.

[25] Wang, P., and Bai, X., 2005, "Large Eddy Simulations of Turbulent Swirling Flows in a Dump Combustor: A Sensitivity Study," Int. J. Numer. Methods Fluids, **47**(2), pp. 99–120.

[26] Freitag, M., Klein, M., Gregor, M., Geyer, D., Schneider, C., Dreizler, A., and Janicka, J., 2006, "Mixing Analysis of a Swirling Recirculating Flow Using DNS and Experimental Data". Int. J. Heat Fluid Flow, **27**(4), pp. 636–643.

[27] Wegner, B., Maltsev, A., Schneider, C., Sadiki, A., Dreizler, A., and Janicka, J., 2004, "Assessment of Unsteady RANS in Predicting Swirl Flow Instability Based on LES and Experiments," Int. J. Heat Fluid Flow, **25**, pp. 528–536.

[28] ANSYS, 2009, *ANSYS Fluent 12.1 User and Theory Guide*, ANSYS, Inc., Southpointe, PA.

[29] Rose, W., 1962, "A Swirling Round Turbulent Jet: 1—Mean-Flow Measurements," J. Appl. Mech., **29**(4), pp. 615-625.

[30] Chigier, N., and Chervinsky, A., 1967, "Experimental Investigation of Swirling Vortex Motion in Jets," J. Appl. Mech., **34**(2), pp. 443–451.

[31] Read, R., 2008, "Experimental Investigations Into High-Altitude Relight of a Gas Turbine". Ph.D. thesis, University of Cambridge, Cambridge, England.

[32] Gupta, A., and Lilley, D., 1985, *Flowfield Modelling and Diagnostics*, Abacus, Tunbridge Wells, England.